

RESEARCH PAPER



Targeting p21-activated kinase 4 (PAK4) with pyrazolo[3,4-d]pyrimidine derivative SPA7012 attenuates hepatic ischaemia-reperfusion injury in mice

Yuancheng Mao^{a*}, Eun Lee^{b*}, Xiaohui Yang^{c*}, Eun Ju Bae^c, Raok Jeon^b and Byung-Hyun Park^a

^aDepartment of Biochemistry and Research Institute for Endocrine Sciences, Jeonbuk National University Medical School, Jeonju, Republic of Korea; ^bResearch Institute of Pharmaceutical Sciences, College of Pharmacy, Sookmyung Women's University, Seoul, Republic of Korea; ^cSchool of Pharmacy, Jeonbuk National University, Jeonju, Republic of Korea

ABSTRACT

p21-Activated kinase 4 (PAK4), one of the serine/threonine kinases activated by Rho-family GTPases, has been widely studied as an oncogenic protein that is overexpressed in many types of cancers. In our recent study, PAK4 upregulation was observed in mice exhibiting hepatic ischaemia-reperfusion (I/R) and in liver transplantation patients. Liver I/R injury was also attenuated in *Pak4* KO mice. Herein, we report a novel series of pyrazolo[3,4-d]pyrimidine derivatives of type I $1/2$ PAK4 inhibitors. The most potent compound SPA7012 was evaluated to determine the pharmacological potential of PAK4 inhibitor in I/R injury in mice. Mice with I/R injury showed typical patterns of liver damage, as demonstrated by increases in serum levels of aminotransferases and proinflammatory cytokines, hepatocellular necrosis and apoptosis, and inflammatory cell infiltration, relative to sham mice. Conversely, intraperitoneal administration of SPA7012 dramatically attenuated biochemical and histopathologic changes. Mechanistically, stabilisation of nuclear factor-erythroid 2-related factor 2 (Nrf2), a master regulator of anti-oxidative response, was observed following SPA7012 treatment. SPA7012 treatment in primary hepatocytes also attenuated hypoxia-reoxygenation-induced apoptotic cell death and inflammation. Together, these results provide experimental evidence supporting the use of PAK4 inhibitors for alleviation of I/R-induced liver damage.

Abbreviations: I/R: ischaemia-reperfusion; H/R: hypoxia-reoxygenation; PAK4: p21-activated kinase 4; Nrf2: nuclear factor-erythroid 2-related factor 2; Keap1: Kelch-like ECH-associated protein 1; HO-1: haem oxygenase-1; NQO1: NAD(P)H quinone oxidoreductase 1; GPx: glutathione peroxidase; ALT: alanine aminotransferase; AST: aspartate aminotransferase; GSH: glutathione; MAD: malondialdehyde; LDH: lactate dehydrogenase; Co-IP: co-immunoprecipitation

ARTICLE HISTORY

Received 31 March 2022
Revised 15 July 2022
Accepted 21 July 2022

KEYWORDS

PAK4; pyrazolo[3,4-d]pyrimidine; liver; ischaemia-reperfusion; hypoxia-reoxygenation; Nrf2

1. Introduction

Hepatic ischaemia/reperfusion (I/R) injury following surgical procedures such as liver tumour resection and liver transplantation is a major cause of liver dysfunction and even liver failure.¹ The primary pathogenic mechanism of hepatic I/R injury is cell death and inflammation. The initial hypoxic injury due to the interruption of blood flow causes parenchymal cell death.² During the reperfusion period, the return of blood flow further aggravates liver injury due to an inflammatory response, including macrophage and neutrophil infiltration, and cytokine/chemokine production.³ These events together with reoxygenation produce reactive oxygen species (ROS), contributing to further cellular dysfunction and damage.

To protect against ROS-induced tissue damage, liver cells develop defense mechanisms including coordinated induction of various antioxidant proteins. NF-E2-related factor 2 (Nrf2) is a prime example of this response.^{4,5} Under basal conditions, Nrf2 is sequestered in the cytoplasm by binding to its repressor, Kelch-like ECH-associated protein 1 (Keap1). Oxidative stress modifies

cysteine residues of Keap1, resulting in dissociation of Nrf2 from Keap1 and subsequent translocation from the cytoplasm to the nucleus. Nuclear Nrf2 binds to the antioxidant response element (ARE) present in the promoter regions of antioxidant enzymes, such as haem oxygenase-1 (HO-1), NAD(P)H quinone oxidoreductase 1 (NQO1), and glutathione peroxidase (GPx).⁶ In this process, multiple protein kinases participate in the subcellular localisation of Nrf2 and its protein stability. For example, protein kinase C, casein kinase 2, and AMP-activated kinase phosphorylate different regions of Nrf2 and promote nuclear translocation of Nrf2. Conversely, glycogen synthase kinase 3 β and Fyn-mediated phosphorylation shift the subcellular distribution of Nrf2 towards the cytoplasm where it is degraded via the ubiquitin-proteasome pathway.^{7,8} Recently, we have reported that p21-activated kinase 4 (PAK4), an oncogenic protein, phosphorylates Nrf2 at T369 and exports Nrf2 from the nucleus to the cytoplasm.⁹ In contrast, genetic deletion of *Pak4* increases protein stability of Nrf2 and suppresses oxidative stress. These results indicate that PAK4 inhibition

CONTACT Eun Ju Bae  ejbae7@jbnu.ac.kr  School of Pharmacy, Jeonbuk National University, Jeonju 54896, Republic of Korea; Raok Jeon  rjeon@sookmyung.ac.kr  College of Pharmacy, Sookmyung Women's University, Cheongpa-ro 47-gil 100, Yongsan-gu, Seoul 04310, Republic of Korea; Byung-Hyun Park  bhpark@jbnu.ac.kr  Department of Biochemistry and Research Institute for Endocrine Sciences, Jeonbuk National University Medical School, Jeonju 54896, Republic of Korea

*These authors contributed equally to this work.

© 2022 The Author(s). Published by Informa UK Limited, trading as Taylor & Francis Group.

This is an Open Access article distributed under the terms of the Creative Commons Attribution License (<http://creativecommons.org/licenses/by/4.0/>), which permits unrestricted use, distribution, and reproduction in any medium, provided the original work is properly cited.

is an effective way to enable the Nrf2-mediated antioxidant response to protect mice from I/R injury.

Several PAK4 inhibitors have been described over the last decade. PF-3758309 was first developed by Pfizer as a pan-PAK inhibitor through structure-based design combined with high-throughput screening and displayed anti-tumour effects against several types of cancers.^{10,11} PF-3758309 was evaluated in clinical trials (NCT00932126); however, further investigation was terminated due to undesirable pharmacokinetic properties and poor bioavailability.¹² A second compound, KPT-9274, a dual inhibitor of PAK4 and nicotinamide phosphoribosyltransferase,¹³ is currently in clinical trials (NCT02702492) for the treatment of patients with refractory/relapsed haematologic and solid tumours. Recently, Guo et al. developed PAK4 inhibitor as a prodrug form (CZH-226) and observed improved pharmacokinetic and tissue distribution and well tolerability in a rat model of cancers.^{13,14} Unfortunately, use of the aforementioned PAK4 inhibitors has been limited by their weak potency and lack of PAK4 selectivity. Based on our previous study confirming PAK4 as a negative regulator of Nrf2-ARE pathways,⁹ we closely examined our newly identified PAK4-specific inhibitor SPA7012 for application as a therapeutic for the treatment of hepatic I/R injury. We further examined the molecular basis underlying the protective activities of this small molecule against oxidative stress in cultured hepatocytes with hypoxia-reoxygenation (H/R) and in mice with hepatic I/R.

2. Experimental section

2.1. Chemistry

2.1.1. General

Most reagents and solvents were purchased from commercial sources and used without further purification. All reactions were performed within a nitrogen or argon atmosphere with anhydrous solvents. To monitor the reaction, thin-layer chromatography was performed using Kieselgel 60 F254 plates (Merk Millipore, MA, USA). Flash column chromatography was performed using silica gel 60 (230–400 mesh, Merck Millipore) with the indicated solvents. Medium pressure liquid chromatography was performed with Combiflash® Rf 200 with RediSep Rf columns (Teledyne ISO, Hunt Valley, MD, USA). NMR spectra were recorded on a Varian YH 400 spectrometer (¹H 400 MHz, ¹³C 100 MHz, Agilent, Palo Alto, CA, USA) and an Avance III HD 500 spectrometer (¹H 500 MHz, ¹³C 125 MHz, Bruker, Billerica, MA, USA). Chemical shifts are expressed as δ units using tetramethylsilane as the external standard.

2.1.2. Synthesis

2.1.2.1. 2-(1-Methoxyethylidene)malononitrile¹. A mixture of malononitrile (5.0 mL, 78.60 mmol) and trimethyl orthoacetate (11.0 mL, 86.46 mmol) was heated to reflux for 4 h. After cooling to room temperature, the reaction mixture was purified using MPLC with a gradient of 0–30% EtOAc in *n*-hexane to provide compound **2** (9.51 g, 99%) as a light yellow liquid: $R_f=0.30$ (*n*-hexane:EtOAc = 3:2); ¹H NMR (400 MHz, CDCl₃) δ 4.08 (s, 3H), 2.41 (s, 3H); ¹³C NMR (100 MHz, CDCl₃) δ 185.7, 113.2, 111.1, 66.3, 58.6, 17.4.

2.1.2.2. 2-(3-Dimethylamino-1-methoxyallylidene)malononitrile².

To a mixture of compound **1** (9.51 g, 77.86 mmol) in MeOH (120 mL), DMF-DMA (11.7 mL, 85.65 mmol) was added. The reaction mixture was heated at reflux for 1 h. After cooling to room temperature, the reaction mixture was concentrated and diluted

with water. The resulting mixture was extracted with dichloromethane (DCM). The combined organic layers were washed with brine and dried over MgSO₄, filtered, and concentrated *in vacuo*. The residue was recrystallised (EtOH 100%) and purified by flash column chromatography to provide compound **3** (14.60 g, 67%) as a brown solid: $R_f=0.19$ (*n*-hexane:EtOAc = 1:1); ¹H NMR (400 MHz, CDCl₃) δ 7.55 (d, $J=12.3$ Hz, 1H), 5.09 (d, $J=12.3$ Hz, 1H), 4.10 (s, 3H), 3.21 (s, 3H), 2.95 (s, 3H); ¹³C NMR (100 MHz, CDCl₃) δ 181.7, 152.8, 117.4, 116.1, 87.4, 60.7, 45.8, 37.4.

2.1.2.3. 2-Bromo-4-methoxynicotinonitrile³. To a mixture of compound **2** (2.30 g, 12.96 mmol) in 48% HBr (26 mL), acetic acid glacial (13 mL) was added. After stirring for 14 h at room temperature, the reaction mixture was neutralised with NaHCO₃ (aq) and extracted with EtOAc. The combined organic layers were washed with brine and dried over MgSO₄, filtered, and concentrated *in vacuo*. The residue was purified by medium pressure liquid chromatography (MPLC) with a gradient of 0–40% EtOAc in *n*-hexane to provide compound **3** (1.81 g, 66%) as a yellow solid: $R_f=0.30$ (*n*-hexane:EtOAc = 1:1); ¹H NMR (400 MHz, CDCl₃) δ 8.40 (d, $J=5.9$ Hz, 1H), 6.92 (d, $J=5.9$ Hz, 1H), 4.03 (s, 3H); ¹³C NMR (100 MHz, CDCl₃) δ 168.7, 153.5, 145.3, 113.3, 106.1, 103.8, 57.0.

2.1.2.4. 4-Hydroxy-1H-pyridin-2-one⁴. A reaction tube was charged with concentrated hydrochloric acid (HCl) (6 mL) solution and then compound **3** (1.38 g, 6.48 mmol) was added. The tube was sealed, and the mixture was heated at 160 °C for 15 h. After cooling to room temperature, the reaction mixture was diluted with water and neutralised with 2 N NaOH (aq). The resulting mixture was dried over reduced pressure and dissolved in MeOH. The resulting suspension was filtered, and the filtrate was purified by MPLC with a gradient of 0–20% MeOH in CHCl₃ to provide compound **4** (676 mg, 94%) as a white solid: $R_f=0.22$ (CHCl₃:MeOH = 8:1); ¹H NMR (400 MHz, DMSO-*d*₆) δ 11.07 (s, 1H), 7.26 (d, $J=7.2$ Hz, 1H), 5.88 (d, $J=7.2$ Hz, 1H), 5.60 (s, 1H), 3.12 (s, 1H); ¹³C NMR (100 MHz, DMSO-*d*₆) δ 168.5, 164.9, 136.2, 100.5, 99.1.

2.1.2.5. 2,5-Dihydropyrido[4,3-*b*]indolone⁵. To a mixture of compound **4** (312 mg, 2.81 mmol) in diphenyl ether (28 mL), phenylhydrazine (0.34 mL, 3.37 mmol) was added. The reaction mixture was heated at reflux in a pre-heated sand bath and stirred for 18 h. After cooling to room temperature, the reaction mixture was poured onto *n*-hexane (300 mL). The precipitate was filtered and rinsed with tetrahydrofuran (THF). The combined filtrate was purified by flash column chromatography to provide **5** (101 mg, 20%) as a brown solid: $R_f=0.33$ (CHCl₃:MeOH = 8:1); ¹H NMR (400 MHz, CD₃OD) δ 8.22 (d, $J=7.8$ Hz, 1H), 7.47 (d, $J=8.1$ Hz, 1H), 7.36 (d, $J=7.1$ Hz), 7.34 (t, $J=8.1$ Hz, 1H), 7.24 (t, $J=7.8$ Hz, 1H), 6.68 (d, $J=7.1$ Hz, 1H).

2.1.2.6. 1-Chloro-5H-pyrido[4,3-*b*]indole⁶. A mixture of compound **5** (648 mg, 3.52 mmol) and phosphorous oxychloride (10 mL) was heated to reflux for 14 h. After cooling to room temperature, the reaction mixture was concentrated, neutralised with NaHCO₃ (aq) and extracted with DCM. The combined organic layers were washed with brine and dried over MgSO₄, filtered, and concentrated *in vacuo*. The residue was purified by flash column chromatography to provide compound **6** (376 mg, 53%) as a pale yellow solid: $R_f=0.51$ (CHCl₃:MeOH = 10:1); ¹H NMR (500 MHz, DMSO-*d*₆) δ 12.15 (s, 1H), 8.38 (d, $J=7.9$ Hz, 1H), 8.24 (d, $J=5.6$ Hz, 1H), 7.65 (d, $J=7.5$ Hz, 1H), 7.57 (t, $J=7.5$ Hz, 1H), 7.54 (d, $J=5.6$ Hz, 1H),

7.37 (t, $J=7.9$ Hz, 1H); ^{13}C NMR (125 MHz, DMSO- d_6) δ 145.9, 144.2, 144.1, 140.1, 127.7, 122.4, 121.1, 120.0, 116.7, 112.3, 107.0.

2.1.2.7. 4-Methoxybenzyl(5H-pyrido[4,3-b]indol-1-yl)amine⁷. A reaction tube was charged with compound **6** (407 mg, 2.01 mmol) and 4-methoxybenzylamine (5.3 mL, 40.12 mmol). The tube was sealed, and the mixture was heated at 200 °C for 4 h. After cooling to room temperature, the reaction mixture was diluted with water and extracted with EtOAc. The combined organic layers were washed with brine and dried over MgSO_4 , filtered, and concentrated *in vacuo*. The residue was purified by flash column chromatography to provide compound **7** (760 mg, quantitative) as a pale yellow solid: $R_f=0.32$ (*n*-hexane:EtOAc = 1:1); ^1H NMR (400 MHz, CDCl_3) δ 8.76 (s, 1H), 8.12 (dd, $J=5.6$, 2.0 Hz, 1H), 7.76 (d, $J=8.0$ Hz, 1H), 7.49–7.33 (m, 3H), 7.30–7.20 (m, 2H), 6.96–6.84 (m, 2H), 6.78 (dd, $J=5.6$, 2.0 Hz, 1H), 5.13 (s, 1H), 4.87 (d, $J=3.2$ Hz, 2H), 3.80 (s, 3H).

2.1.2.8. (5-(3-Bromophenyl)-5H-pyrido[4,3-b]indolyl)(4-methoxybenzyl)amine⁸. To a mixture of compound **7** (674 mg, 2.22 mmol), copper powder (283 mg, 4.45 mmol), potassium carbonate (922 mg, 6.67 mmol), 18-crown-6 (178 mg, 0.67 mmol) in 1,2-dichlorobenzene (10 mL), was added 3-bromo-1-iodobenzene (434 μL , 3.33 mmol). The reaction mixture was heated at 180 °C for 5 h. The hot reaction mixture was filtered through a celite pad and rinsed with hot EtOAc. The combined filtrate was washed with brine and dried over MgSO_4 , filtered, and concentrated *in vacuo*. The residue was purified by flash column chromatography to provide compound **8** (436 mg, 43%) as a yellow solid: $R_f=0.63$ (*n*-hexane:EtOAc = 2:1); ^1H NMR (400 MHz, CDCl_3) δ 8.12 (s, 1H), 7.81 (s, 1H), 7.72–7.58 (m, 2H), 7.52–7.27 (m, 7H), 6.92 (d, $J=6.8$ Hz, 2H), 6.70 (s, 1H), 5.19 (s, 1H), 4.87 (s, 2H), 3.81 (s, 3H).

2.1.2.9. 5-(3-Bromophenyl)-5H-pyrido[4,3-b]indolylamine⁹. A mixture of compound **8** (391 mg, 0.85 mmol) and trifluoroacetic acid (3.3 mL) was heated to 60 °C for 30 min. After cooling to room temperature, the reaction mixture was poured onto ice water, neutralised with NaHCO_3 (aq) and extracted with EtOAc. The combined organic layers were washed with brine and dried over MgSO_4 , filtered, and concentrated *in vacuo*. The residue was purified by flash column chromatography to provide compound **9** (336 mg, quantitative) as a pale yellow solid: $R_f=0.11$ (*n*-hexane:EtOAc = 1:1); ^1H NMR (400 MHz, CDCl_3) δ 8.00 (d, $J=5.6$ Hz, 1H), 7.92 (d, $J=7.2$ Hz, 1H), 7.67 (s, 1H), 7.63 (d, $J=7.2$ Hz, 1H), 7.53–7.28 (m, 5H), 6.72 (t, $J=5.2$ Hz, 1H), 5.47 (s, 2H).

2.1.2.10. General procedures for the synthesis of compounds 10a–c, 14a–d and 18a–b. To a mixture of compound **9**, **13** or **17** (1.0 equiv.) in TEA/DMSO (2:1) was added bis(triphenylphosphine) palladium(II) dichloride (1.0 equiv.) under a nitrogen atmosphere. After stirring at room temperature for 10 min, alkyl acetylene (10.0 equiv.) was added. The reaction mixture was heated at 70 °C for 1 h. After cooling to room temperature, the mixture was filtered through a celite pad and rinsed with EtOAc. Water was added to the filtrate and the mixture was extracted with EtOAc. The combined organic layers were dried over MgSO_4 , filtered, and concentrated *in vacuo*. The residue was purified by flash column chromatography (CHCl_3 :EtOAc or EtOAc:MeOH) to provide compounds **10**, **14** or **18**.

2.1.2.11. 4-(3-(1-Aminopyrido[4,3-b]indol-5-yl)phenyl)-2-methylbutyn-2-ol (10a). Off-white solid (71%): $R_f=0.31$ (EtOAc 100%); ^1H

NMR (400 MHz, CDCl_3) δ 7.97 (d, $J=5.8$ Hz, 1H), 7.87 (d, $J=7.9$ Hz, 1H), 7.54–7.48 (m, 3H), 7.40–7.31 (m, 4H), 6.67 (d, $J=5.8$ Hz, 1H), 5.35 (s, 2H), 3.56 (s, 1H), 1.65 (s, 6H); ^{13}C NMR (100 MHz, CDCl_3) δ 153.9, 146.4, 143.5, 139.8, 136.6, 131.3, 130.0, 129.9, 126.8, 125.2, 125.0, 121.8, 121.4, 120.3, 110.0, 104.2, 97.8, 96.0, 80.6, 65.2, 31.4; HRMS m/z : 342.1614 $[\text{M} + \text{H}]^+$; calculated $\text{C}_{22}\text{H}_{20}\text{N}_3\text{O}^+$: 342.1606.

2.1.2.12. 3-(1-Aminopyrido[4,3-b]indol-5-yl)phenylethynylcyclohexan-1-ol (10b). Yellow solid (49%): $R_f=0.38$ (EtOAc 100%); ^1H NMR (500 MHz, CDCl_3) δ 7.99 (d, $J=5.9$ Hz, 1H), 7.90 (d, $J=7.6$ Hz, 1H), 7.60–7.51 (m, 3H), 7.46–7.33 (m, 4H), 6.71 (d, $J=5.9$ Hz, 1H), 5.42 (s, 2H), 4.01 (s, 1H), 2.07–1.99 (m, 2H), 1.80–1.53 (m, 7H), 1.35–1.24 (m, 1H); ^{13}C NMR (125 MHz, CDCl_3) δ 153.9, 146.5, 143.3, 139.9, 136.7, 131.5, 130.1, 130.0, 127.0, 125.3, 125.2, 121.8, 121.6, 120.4, 110.1, 104.3, 98.0, 94.9, 82.9, 68.9, 40.0, 25.2, 23.4; HRMS m/z : 382.1930 $[\text{M} + \text{H}]^+$; calculated $\text{C}_{25}\text{H}_{24}\text{N}_3\text{O}^+$: 382.1919.

2.1.2.13. 4-(3-(1-Aminopyrido[4,3-b]indol-5-yl)phenyl)-2-methylbutyn-1,2-diol (10c). Off-white solid (10%): $R_f=0.16$ (EtOAc 100%); ^1H NMR (500 MHz, CD_3OD) δ 8.24 (d, $J=7.5$ Hz, 1H), 7.88 (d, $J=6.1$ Hz, 1H), 7.70–7.63 (m, 3H), 7.55 (dt, $J=7.0$, 2.1 Hz, 1H), 7.49–7.36 (m, 3H), 6.73 (d, $J=6.1$ Hz, 1H), 3.61 (s, 2H); ^{13}C NMR (125 MHz, CD_3OD) δ 154.1, 146.5, 141.9, 139.8, 136.6, 131.3, 130.1, 129.8, 126.9, 125.2, 125.1, 121.8, 121.5, 120.6, 109.5, 103.8, 97.0, 93.3, 81.7, 69.6, 68.2, 24.7; HRMS m/z : 358.1561 $[\text{M} + \text{H}]^+$; calculated $\text{C}_{22}\text{H}_{20}\text{N}_3\text{O}_2^+$: 358.1556.

2.1.2.14. 5-Amino-3-methyl-1H-pyrazole-4-carbonitrile¹¹. To a solution of compound **1** (1.64 g, 13.42 mmol) in EtOH (25 mL), hydrazine monohydrate (1.3 mL, 26.84 mmol) was added. The reaction mixture was heated at 80 °C for 1 h. After cooling to room temperature, the reaction mixture was concentrated. The residue was purified by flash column chromatography to provide compound **11** (1.60 g, 98%) as an off-white solid: $R_f=0.31$ (*n*-hexane:EtOAc = 1:2); ^1H NMR (500 MHz, CD_3OD) δ 2.25 (s, 3H).

2.1.2.15. 3-Methyl-1H-pyrazolo[3,4-d]pyrimidin-4-ylamine¹². A mixture of compound **11** (1.37 g, 11.22 mmol) and formamide (9 mL) was heated to 180 °C for 18 h. After cooling to room temperature, the reaction mixture was poured into water and cooled via ice bath. The solid was filtered and rinsed with water and MeOH to provide compound **12** (1.10 g, 65%) as a yellow solid without further purification: $R_f=0.26$ (EtOAc:MeOH = 10:1); ^1H NMR (500 MHz, CD_3OD) δ 8.15 (s, 1H), 2.62 (s, 3H); ^{13}C NMR (125 MHz, CD_3OD) δ 164.7, 159.0, 155.5, 152.0, 98.6, 12.9.

2.1.2.16. General procedures for the synthesis of compounds 13 and 17a–b. To a mixture of compound **12** or **16** (1.0 equiv.), copper(I) iodide (0.2 equiv.), potassium carbonate (2.0 equiv.) in DMF, DMEDA (0.4 equiv.) and 3-bromo-1-iodobenzene (1.2 equiv.) were added. The reaction mixture was heated at 110 °C for 3 to 23 h. After cooling to room temperature, the reaction mixture was filtered through a celite pad and rinsed with EtOAc. The combined filtrate was washed with brine and dried over MgSO_4 , filtered, and concentrated *in vacuo*. The residue was purified by flash column chromatography (EtOAc:MeOH) to provide compound **13** or **17**.

2.1.2.17. (3-Bromophenyl)-3-methyl-1H-pyrazolo[3,4-d]pyrimidin-4-ylamine¹³. Off-white solid (25%): $R_f=0.67$ (EtOAc:MeOH = 10:1); ^1H NMR (500 MHz, CD_3OD) δ 8.40 (s, 1H), 8.28 (s, 1H), 8.18 (d, $J=8.0$ Hz, 1H), 7.49–7.40 (m, 2H), 2.69 (s, 3H); ^{13}C NMR (125 MHz,

CD₃OD) δ 158.9, 156.2, 154.4, 143.8, 142.2, 140.0, 130.2, 128.6, 123.5, 122.0, 119.4, 13.1.

2.1.2.18. *4-(3-(4-Amino-3-methylpyrazolo[3,4-d]pyrimidin-1-yl)phenyl)-2-methylbutyn-2-ol (14a, SPA7011)*. Pale yellow solid (58%): $R_f = 0.29$ (CHCl₃:EtOAc = 1:3); ¹H NMR (500 MHz, CD₃OD) δ 8.26 (s, 1H), 8.18 (s, 1H), 8.08 (d, $J = 8.2$ Hz, 1H), 7.48 (t, $J = 8.0$ Hz, 1H), 7.36 (d, $J = 7.7$ Hz, 1H), 2.69 (s, 3H), 1.61 (s, 6H); ¹³C NMR (125 MHz, CD₃OD) δ 158.9, 156.1, 154.1, 143.5, 138.8, 128.8, 123.9, 123.8, 120.9, 100.5, 94.5, 80.5, 64.5, 30.3, 13.1; HRMS m/z : 308.1513 [M + H]⁺; calculated C₁₇H₁₈N₅O⁺: 308.1511.

2.1.2.19. *3-(4-Amino-3-methylpyrazolo[3,4-d]pyrimidin-1-yl)phenylethynylcyclohexan-1-ol (14b, SPA7012)*. Pale yellow solid (85%): $R_f = 0.33$ (CHCl₃:EtOAc = 1:3); ¹H NMR (500 MHz, CD₃OD) δ 8.14 (s, 1H), 8.06 (s, 1H), 7.98 (d, $J = 8.0$ Hz, 1H), 7.37 (dd, $J = 8.0, 7.7$ Hz, 1H), 7.26 (d, $J = 7.7$ Hz, 1H), 2.57 (s, 3H), 1.96–1.84 (m, 2H), 1.71–1.45 (m, 7H), 1.29–1.16 (m, 1H); ¹³C NMR (125 MHz, CD₃OD) δ 158.9, 156.1, 154.2, 143.5, 138.8, 128.9, 128.8, 124.0, 123.8, 120.9, 100.5, 93.6, 68.0, 39.5, 25.0, 23.0, 13.1; HRMS m/z : 348.1827 [M + H]⁺; calculated C₂₀H₂₂N₅O⁺: 348.1824

2.1.2.20. *4-(3-(4-Amino-3-methylpyrazolo[3,4-d]pyrimidin-1-yl)phenyl)-2-methylbutyn-1,2-diol (14c, SPA7013)*. Yellow solid (82%): $R_f = 0.13$ (CHCl₃:EtOAc = 1:3); ¹H NMR (500 MHz, CD₃OD) δ 8.26 (s, 1H), 8.21 (s, 1H), 8.09 (d, $J = 8.0$ Hz, 1H), 7.48 (dd, $J = 8.0, 7.8$ Hz, 1H), 7.40 (d, $J = 7.8$ Hz, 1H), 3.63 (s, 2H), 2.69 (s, 3H), 1.56 (s, 3H); ¹³C NMR (125 MHz, CD₃OD) δ 156.1, 143.5, 138.8, 129.0, 128.8, 123.9, 123.8, 121.0, 92.2, 82.4, 69.7, 68.2, 60.1, 24.8, 19.4, 13.1; HRMS m/z : 324.1471 [M + H]⁺; calculated C₁₇H₁₈N₅O₂⁺: 324.1461.

2.1.2.21. *4-(3-(4-Amino-3-methylpyrazolo[3,4-d]pyrimidin-1-yl)phenyl)-2-phenylbutyn-2-ol (14d, SPA7014)*. Pale yellow solid (46%): $R_f = 0.33$ (CHCl₃:EtOAc = 1:5); ¹H NMR (500 MHz, CD₃OD) δ 8.26 (s, 1H), 8.24 (t, $J = 1.6$ Hz, 1H), 8.12 (dd, $J = 8.2, 1.0$ Hz, 1H), 7.76–7.71 (m, 2H), 7.51 (t, $J = 7.9$ Hz, 1H), 7.46–7.37 (m, 3H), 7.31 (d, $J = 7.4$ Hz, 1H), 2.70 (s, 3H), 1.85 (s, 3H); ¹³C NMR (125 MHz, CD₃OD) δ 158.9, 156.1, 154.1, 146.0, 143.6, 138.9, 128.9, 128.8, 127.8, 127.1, 124.7, 123.8, 123.7, 121.1, 100.5, 93.6, 83.0, 69.3, 32.5, 13.1 HRMS m/z : 370.1679 [M + H]⁺; calculated C₂₂H₂₀N₅O⁺: 370.1668.

2.1.2.22. General procedures for the synthesis of compounds 15a–b. *Step 1.* To a mixture of methanesulfonyl chloride (1.2 equiv.) in DCM, was slowly added propargyl alcohol (1.0 equiv.) and triethylamine (1.2 equiv.), simultaneously. The reaction mixture was stirred at room temperature for 1 h. The reaction mixture was washed with water and dried over MgSO₄, filtered, and concentrated to provide methanesulfonic acid prop-2-ynyl ester as a yellow liquid without further purification. *Step 2.* To a mixture of methanesulfonic acid prop-2-ynyl ester in DCM, was added morpholine or piperidine (2.0 equiv.). After stirring at room temperature for 4 to 12 h, the reaction mixture was filtered. The combined filtrate was washed with NaHCO₃ (aq) and dried over MgSO₄, filtered, and concentrated *in vacuo*. The crude intermediates were used for the next step without further purification. *Step 3.* To a mixture of 3-Iodo-1H-pyrazolo[3,4-d]pyrimidin-4-amine (1.0 equiv.) and copper(II) iodide (0.2 equiv.) in DMF, was added tetrakis (triphenylphosphine)palladium(0) (0.1 equiv.) under a nitrogen atmosphere. After stirring at room temperature for 10 min, triethylamine (2.0 equiv.) and propargyl morpholine or propargyl piperidine (10.0 equiv.) were added. The reaction mixture was

heated at 70 °C for 1.5 h. After cooling to room temperature, the mixture was filtered through a celite pad and rinsed with EtOAc. Water was added to the filtrate and the mixture was extracted with EtOAc. The combined organic layers were dried over MgSO₄, filtered, and concentrated *in vacuo*. The residue was purified by flash column chromatography (EtOAc: MeOH) to provide compound **15**.

2.1.2.23. *3-(3-Morpholin-4-ylprop-1-ynyl)-1H-pyrazolo[3,4-d]pyrimidin-4-ylamine (15a)*. Pale yellow solid (47%): $R_f = 0.22$ (DCM:MeOH = 6:1); ¹H NMR (500 MHz, CD₃OD) δ 8.10 (s, 1H), 3.72–3.60 (m, 4H), 3.54 (s, 2H), 2.59 (br s, 4H).

2.1.2.24. *3-(3-Piperidin-1-ylprop-1-ynyl)-1H-pyrazolo[3,4-d]pyrimidin-4-ylamine (15b)*. Pale yellow solid (47%): $R_f = 0.22$ (EtOAc:MeOH = 4:1); ¹H NMR (500 MHz, CD₃OD) δ 8.21 (s, 1H), 3.61 (s, 2H), 2.68 (br s, 4H), 1.74–1.65 (m, 4H), 1.53 (br s, 2H).

2.1.2.25. General procedures for the synthesis of compounds 16a–b. To a mixture of compound **15** (1.0 equiv.) in MeOH, Pd/C (50 wt%) was added and the reaction mixture was then stirred within a hydrogen atmosphere for 1.5 h. The mixture was filtered through a celite pad, rinsed with MeOH, and concentrated *in vacuo*. The residue was purified by flash column chromatography (EtOAc:MeOH) to provide compound **16**.

2.1.2.26. *3-(3-Morpholin-4-ylpropyl)-1H-pyrazolo[3,4-d]pyrimidin-4-ylamine (16a)*. White solid (61%): $R_f = 0.15$ (EtOAc:MeOH = 4:1); ¹H NMR (500 MHz, CD₃OD) δ 8.18 (s, 1H), 3.70 (t, $J = 4.6$ Hz, 4H), 3.03 (t, $J = 7.1$ Hz, 2H), 2.53–2.40 (m, 6H), 1.98 (quint., $J = 7.1$ Hz, 2H).

2.1.2.27. *3-(3-Piperidin-1-ylpropyl)-1H-pyrazolo[3,4-d]pyrimidin-4-ylamine (16b)*. Yellow solid (97%): $R_f = 0.04$ (EtOAc:MeOH = 4:1); ¹H NMR (500 MHz, CD₃OD) δ 8.16 (s, 1H), 3.02 (t, $J = 7.2$ Hz, 2H), 2.58–2.27 (m, 6H), 1.98 (quint., $J = 7.2$ Hz, 2H), 1.68–1.59 (m, 4H), 1.50 (br s, 2H).

2.1.2.28. *1-(3-Bromophenyl)-3-(3-morpholin-4-ylpropyl)-1H-pyrazolo[3,4-d]pyrimidin-4-ylamine (17a)*. White solid (57%): $R_f = 0.30$ (EtOAc:MeOH = 4:1); ¹H NMR (500 MHz, CD₃OD) δ 8.30 (t, $J = 1.9$ Hz, 1H), 8.18 (s, 1H), 8.09 (dt, $J = 8.1, 1.9$ Hz, 1H), 7.37–7.29 (m, 2H), 3.61 (t, $J = 5.0$ Hz, 4H), 3.00 (t, $J = 7.1$ Hz, 2H), 2.50–2.38 (m, 6H), 1.98 (quint., $J = 7.1$ Hz, 2H).

2.1.2.29. *1-(3-Bromophenyl)-3-(3-piperidin-1-ylpropyl)-1H-pyrazolo[3,4-d]pyrimidin-4-ylamine (17b)*. White solid (52%): $R_f = 0.14$ (EtOAc:MeOH = 4:1); ¹H NMR (500 MHz, CD₃OD) δ 8.43 (t, $J = 1.9$ Hz, 1H), 8.30 (s, 1H), 8.24–8.20 (m, 1H), 7.51–7.42 (m, 2H), 3.10 (t, $J = 7.2$ Hz, 2H), 2.59–2.44 (m, 6H), 2.09 (quint., $J = 7.2$ Hz, 2H), 1.70–1.61 (m, 4H), 1.52 (br s, 2H).

2.1.2.30. *3-(4-Amino-3-(3-morpholin-4-ylpropyl)pyrazolo[3,4-d]pyrimidin-1-yl)phenylethynylcyclohexanol (18a, SPA7016)*. Off-white solid (66%): $R_f = 0.33$ (EtOAc:MeOH = 4:1); ¹H NMR (500 MHz, CD₃OD) δ 8.28 (s, 1H), 8.20 (t, $J = 2.0$ Hz, 1H), 8.14 (ddd, $J = 8.0, 2.0, 1.0$ Hz, 1H), 7.50 (t, $J = 8.0$ Hz, 1H), 7.38 (dt, $J = 8.0, 1.0$ Hz, 1H), 3.72 (t, $J = 4.6$ Hz, 4H), 3.12 (t, $J = 7.1$ Hz, 2H), 2.58–2.43 (m, 6H), 2.13–1.98 (m, 4H), 1.83–1.59 (m, 7H), 1.35 (br s, 1H); ¹³C NMR (125 MHz, CD₃OD) δ 156.0, 154.1, 146.9, 138.9, 128.8, 124.0, 123.7, 120.8, 100.4, 93.7, 82.9, 68.0, 66.2, 57.0, 53.3, 39.5, 39.0, 25.2, 25.0,

24.9, 23.0, 13.1; HRMS m/z : 461.2666 $[M + H]^+$; calculated $C_{26}H_{33}N_6O_2^+$: 461.2665.

2.1.2.31. (3-[4-Amino-3-(3-piperidin-1-ylpropyl)pyrazolo[3,4-d]pyrimidin-1-yl]phenylethynyl)cyclohexanol (18 b, SPA7017). Off-white solid (40%): $R_f = 0.36$ (EtOAc:MeOH = 4:1); 1H NMR (500 MHz, CD_3OD) δ 8.22 (s, 1H), 8.17 (s, 1H), 8.10 (d, $J = 8.0$ Hz, 1H), 7.43 (dd, $J = 8.0, 7.6$ Hz, 1H), 7.32 (d, $J = 7.6$ Hz, 1H), 3.00 (t, $J = 7.0$ Hz, 2H), 2.48–2.30 (m, 5H), 2.04–1.93 (m, 4H), 1.80–1.37 (m, 14H), 1.28 (s, 1H); HRMS m/z : 459.2875 $[M + H]^+$; calculated $C_{27}H_{35}N_6O^+$: 459.2872.

2.2. Kinase activity assay

To examine the enzyme activity, HotSpot kinase assay was performed at Reaction Biology Corporation (Malvern, PA, USA). The kinase and substrate pairs were prepared in reaction buffer: 20 mM HEPES at pH 7.5, 10 mM $MgCl_2$, 1 mM EGTA, 0.02% Brij 35, 0.02 mg/mL BSA, 0.1 mM Na_3VO_4 , 2 mM DTT, and 1% DMSO. Compounds were added into the kinase reaction mixture and incubated for 20 min. Then, ^{32}P -ATP was introduced to the mixture to initiate the reaction carried out at 10 μ M of ATP concentration. After 2 h at room temperature, the mixture was spotted onto P81 ion exchange paper and kinase activity was then evaluated utilising the filter-binding method. Compounds were tested for single dose enzyme inhibition at a concentration of 20 μ M. For the control compound, staurosporine was tested in a 10-dose IC_{50} mode. To determine the IC_{50} value, the compounds were tested for 10-doses with 3-fold serial dilution starting at 100 μ M.

2.3. Molecular docking analysis

Molecular docking was carried out using Cresset Flare V.5.0 (Litlington, Cambridgeshire, UK). 3D coordinates of the active site were taken from the crystal structure of the human PAK4 in complex with ligands (PDB code 4O0V) from the RCSB Protein Data Bank. The protein structure was prepared and minimised, and the grid box of the binding site was defined according to the clustered ligand. The docking calculations of synthesised compounds were carried out using Flare V.5.0 in normal docking mode.

2.4. Model of partial hepatic I/R injury

Pathogen-free 8 to 10-week old C57BL/6 male mice (Orient Bio, Seoul, Korea) were kept under a 12-h light/dark cycle with controlled humidity of 50% at 22 °C, and had free access to food and water. Hepatic I/R injury was created using the following method.¹⁵ Mice were anaesthetised with ketamine (100 mg/kg) and xylazine (10 mg/kg) by intraperitoneal injection. A midline incision was performed, and an atraumatic clip was placed across the portal vein, hepatic artery, and bile duct just above the right branch. Blood flow was interrupted to the left lateral and median lobes, which represent approximately 70% of the total blood supply to the liver. The liver was kept moist with a gauze soaked in saline, and body temperature was maintained at 37 °C with a warm blanket throughout ischaemia. After 60 min of partial hepatic ischaemia, the clip was removed to initiate reperfusion. The sham mice underwent the same operation without vascular occlusion. After the desired time period of reperfusion, the mice were euthanised by exsanguination under anaesthesia and serum samples were collected. The left lateral and median lobes of the liver were collected and stored at –80 °C until further analysis, or were immediately fixed in 10% formalin. All animal experiments were

performed in accordance with the Guide for the Care and Use of Laboratory Animals published by the US National Institutes of Health (NIH Publication No. 85–23, revised 2011). The study protocol was approved by the Institutional Animal Care and Use Committee of Jeonbuk National University (permit number: JBNU-2019–00122).

2.5. Isolation of primary hepatocytes

Primary hepatocytes were prepared from 8 to 10 week old C57BL/6 male mice by perfusion. After intubation in the inferior vena cava, the liver was perfused with a calcium-free HEPES buffer (10 mM, pH 7.4) for 5 min at a flow rate of 0.35 mL/min, followed by HEPES buffer containing 5 μ g of collagenase IV (Sigma-Aldrich, St. Louis, MO, USA) with 5 mM calcium chloride for 5 min. Hepatocytes were resuspended in DMEM/F12 supplemented with 10% FBS, 10 units/mL penicillin, 10 μ g/mL streptomycin, and 10 nM dexamethasone mixed with 42% Percoll, and then centrifuged for 5 min at 1,300 rpm. The cells were plated at 1×10^6 cells/well in 6-well culture dishes.

2.6. Hypoxia-reoxygenation protocol

Primary hepatocytes were incubated at 37 °C in anaerobic jars (Oxoid, Basingstoke, Hampshire, UK) with oxygen-absorbing packs (AnaeroGen, Oxoid). This method has been shown to achieve controlled oxygen levels below 1%. Following various periods of hypoxia, reoxygenation of cells was initiated by opening the chamber and replacing the hypoxic medium with an oxygenated medium.

2.7. Cell culture and transient transfection

The human embryonic kidney cell line HEK293T was obtained from the American Type Culture Collection (Manassas, VA, USA). For the Nrf2 reporter gene assay, 1 μ g of a plasmid containing a promoter with an ARE driving luciferase expression was used. Exogenous proteins were expressed by transfecting HEK293T cells with 1 μ g of Nrf2 and PAK4 with Lipofectamine 3000 (Invitrogen, Carlsbad, CA, USA). Luciferase activity was measured using a Dual-Luciferase Reporter Assay (Promega, Madison, WI, USA) by Lumat LB 9507 (Berthold, Bad Wildbad, Germany).

2.8. MTT assay for cell viability

Cell viability was determined by analysing the reduction of 3-(4,5-dimethylthiazol-2-yl)-2,5-diphenyltetrazolium bromide (MTT) to formazan.

2.9. Flow cytometry analysis of apoptosis

H/R-induced apoptosis was monitored using the Annexin V-propidium iodide (PI) double-staining kit (BD Biosciences, San Jose, CA, USA) according to the instructions of the manufacturer, allowing quantification by flow cytometry (BD Biosciences). The proportion of apoptotic cells was defined as the percentage of Annexin V-positive cells relative to PI-positive cells.

2.10. Measurement of cellular ROS levels

Intracellular ROS levels were measured using 2',7'-dichlorofluorescein diacetate (DCF-DA), which converts to fluorescent DCF-DA in cells when exposed to ROS. Briefly, after H/R injury, hepatocytes

Table 1. Sequences and accession numbers for primers (forward, FOR; reverse, REV) used in qPCR

Gene	Sequences for primers	Accession no.
<i>Tnfa</i>	FOR: AGGGTCTGGGCCATAGAACT REV: CCACCACGCTCTTCTGTCTAC	NM_013693
<i>Il1b</i>	FOR: GGTCAAAGGTTTGAAGCAG REV: TGTGAAATGCCACCTTTTGA	NM_008361
<i>Il6</i>	FOR: CCACGGCCTTCCCTACTTC REV: TTGGGAGTGGTATCCTCTGTGA	NM_031168
<i>Icam1</i>	FOR: AACAGTTCACCTGCACGGAC REV: GTCACCGTTGTGATCCCTG	NM_010493
<i>Cxcl1</i>	FOR: AATGAGCTGCGCTGTCAGTG REV: TGAGGGCAACACCTTCAAGC	NM_008176
<i>Ccl2</i>	FOR: ACCGACAACAGGAAGTGGAG REV: TGGACGTTTACACACTGGT	NM_009140
<i>Ho1</i>	FOR: AGGTACACATCCAAGCCGAGA REV: CATCACCAGCTTAAAGCCTTCT	NM_010442
<i>Nqo1</i>	FOR: AGGATGGGAGTACTCGAATC REV: TGCTAGAGATGACTCGGAAGG	NM_008706
<i>Nrf2</i>	FOR: CTTTAGTCAGCGACAGAAGGAC REV: AGGCATCTTGTGGGAATGTG	NM_010902
<i>Gapdh</i>	FOR: CGTCCCAGTACAAAATGGT REV: TTGATGGCAACAATCTCCAC	NM_008084

were loaded with 20 μ M DCF-DA (Invitrogen) for 10 min at 37 °C. The DCF fluorescence intensity was measured by fluorescence spectrophotometry with 485 nm excitation and 538 nm emission and expressed as a percentage relative to control.

2.11. Biochemical analysis

Alanine aminotransferase (ALT) and aspartate aminotransferase (AST) in serum (Asan Pharm, Seoul, Korea), glutathione (GSH, Arbour Assays, Ann Arbor, MI, USA), malondialdehyde (MDA, ab118970, Abcam, Cambridge, UK) in liver tissues, and lactate dehydrogenase (LDH, Biovision, Milpitas, CA, USA) in culture medium were analysed using specific kits. Serum levels of IL-1 β , IL-6, TNF- α , and CCL-2 were detected using ELISA kits (all from Invitrogen).

2.12. RNA isolation and qPCR

Total RNA was extracted from frozen liver tissues or primary hepatocytes using TRIzol reagent (Invitrogen). RNA was treated with isopropanol, dried using 70% ethanol, and dissolved in diethyl pyrocarbonate-treated distilled water. First-strand cDNA was generated using the random hexamer primer provided in the first-strand cDNA synthesis kit (Applied Biosystems, Foster City, CA, USA). Specific primers were designed using PrimerBank (<https://pga.mgh.harvard.edu/primerbank>, Table 1). qPCR reactions were performed in a final volume of 10 μ L containing 10 ng reverse-transcribed total RNA, 200 nM forward and reverse primers, and PCR master mixture. qPCR was performed in 384-well plates using an ABI PrismTM 7900HT Sequence Detection System (Applied Biosystems).

2.13. Subcellular fractionation, Western blotting, and co-immunoprecipitation (Co-IP)

Nuclear and cytoplasmic fractions were prepared using the NE-PER Nuclear and Cytoplasmic Extraction kit (Thermo Fisher Scientific, Waltham, MA, USA). Tissue homogenates or cell lysates (15 μ g) were separated by 6–14% SDS-PAGE and transferred to PVDF membranes. After blocking with 5% skim milk, blots were probed with primary antibodies against: PAK4 (G222), p-PAK4

(S474), p-IKK β (S176/180), p-I κ B α (S32), p-p65 (S536), cleaved caspase-3 (Asp175), Bax (Cell Signalling Technology, Beverly, MA, USA), GAPDH (A531), lamin B1(L75), Bcl2(P65), NQO1 (F252) (Bioworld Technology, St Louis Park, MN, USA), NF- κ B p65 (C-20), I κ B α (H-4), IKK β (10A9B6) (Santa Cruz Biotechnology, Dallas, TX, USA), Nrf2 (Proteintech, Rosemont, IL, USA), HO-1 (Enzo Life Sciences, Farmingdale, New York, USA), and p-Thr (Merck KGaA, Darmstadt, Germany). For co-immunoprecipitations, 600 μ g protein was incubated with anti-Nrf2 antibodies (Proteintech, Sankt Leon-Rot, Germany) overnight at 4 °C followed by protein G agarose for 2 h at 4 °C. Blots were probed with antibodies against PAK4, Nrf2, or p-Thr. Immunoreactive bands were detected with a Las-4000 imager (GE Healthcare Life Science, Pittsburgh, PA, USA).

2.14. Histology

Paraffin sections of liver tissue (5 μ m) were stained with haematoxylin and eosin (H&E) for light microscopy. Five random sections were investigated per slide to measure the necrotic area and determine the percentage of apoptotic cells. To measure the necrotic areas, sections were observed under an Axiovert 40 CFL microscope (Carl Zeiss, Oberkochen, Germany) and measured using iSolution DT 36 software (Carl Zeiss). For immunofluorescence staining, after deparaffinisation, sections were immunostained with antibodies against F4/80 (ab6640), Ly6G (ab25377), and 4-hydroxynonenal (4-HNE, ab46545) (all from Abcam). TUNEL staining was performed with commercial kits (Promega). After washing with phosphate buffered saline (PBS), secondary antibodies (Alexa Fluor 488-conjugated goat anti-mouse IgG1 and Alexa Fluor 594-conjugated goat anti-rabbit IgM, Thermo Fisher Scientific) were incubated for 1 h at 37 °C. Sections were counterstained with DAPI.

2.15. Statistical analysis

Data are expressed as the mean \pm standard deviation of the mean (SD). Statistical comparisons were made using one-way analysis of variance followed by Tukey's *post hoc* analysis. The significance of differences between the two groups was determined using Student's unpaired *t*-test. A *p* values of less than 0.05 was considered significant. All analyses were performed using GraphPad Prism 9.3 (San Diego, CA, USA).

3. Results

3.1. Chemistry

Structure-based drug design was performed to identify novel PAK4 selective inhibitors. GNE-2861 is regarded as the most selective and potent PAK4 inhibitor targeting the specific back pocket of PAK4 caused by abnormal R-spine rearrangement.^{16,17} Therefore, we adopted GNE-2861 as a lead for drug design. To find new selective PAK4 inhibitors with improved properties, attempts were made to change the adenine pocket-binding group while maintaining the back pocket targeting group of GNE (Figure 1(A)). Scaffold hopping of adenine mimic monocycle to bicycle or tricycle was performed, expecting an improved log *p* values and easy-to-add solvent-accessible moieties.¹⁸ Following these changes in the adenine pocket-binding group, the bicyclic linker turned to a monocycle to reduce the structural rigidity of the entire compound. *In silico* fragment screening provided heterocyclic scaffolds with structural novelty. Two privileged structures, namely, pyrido[4,3-*b*]indole (used as a synonym of γ -carboline) and

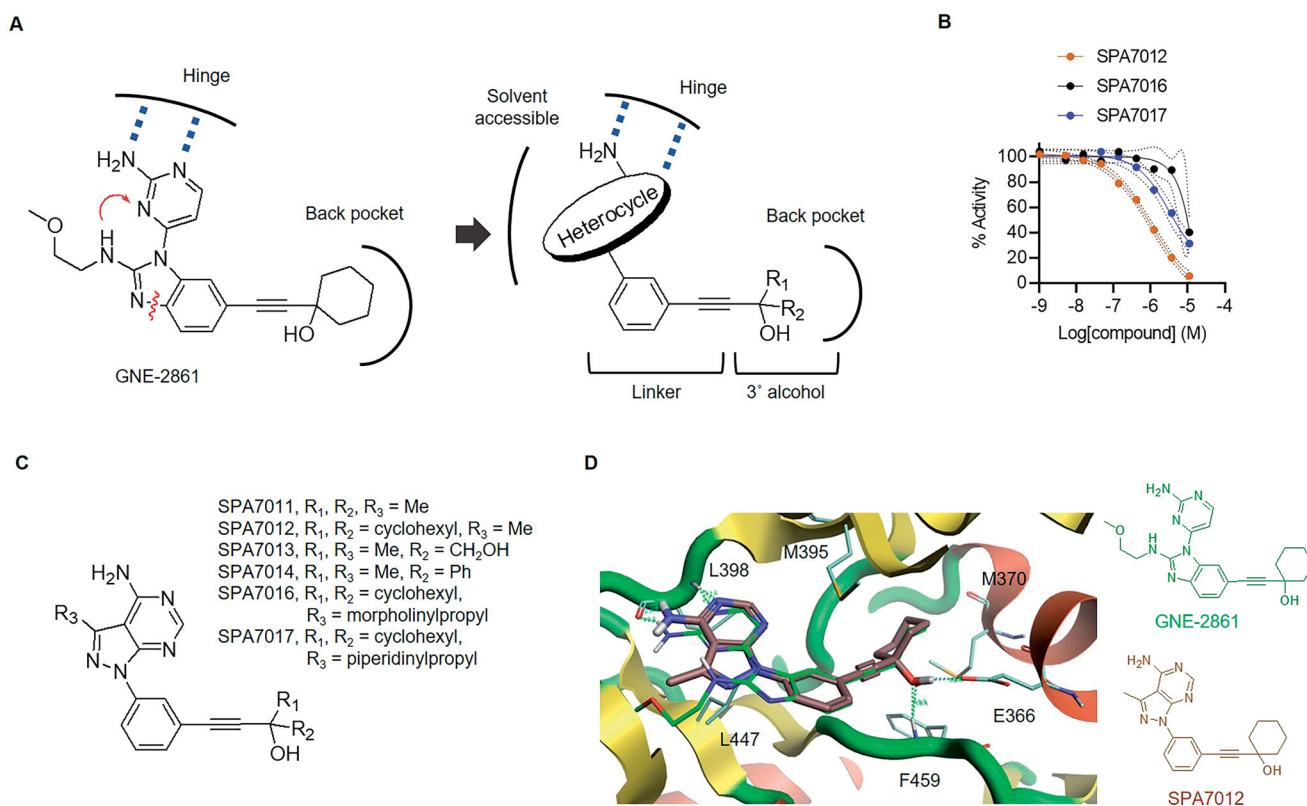
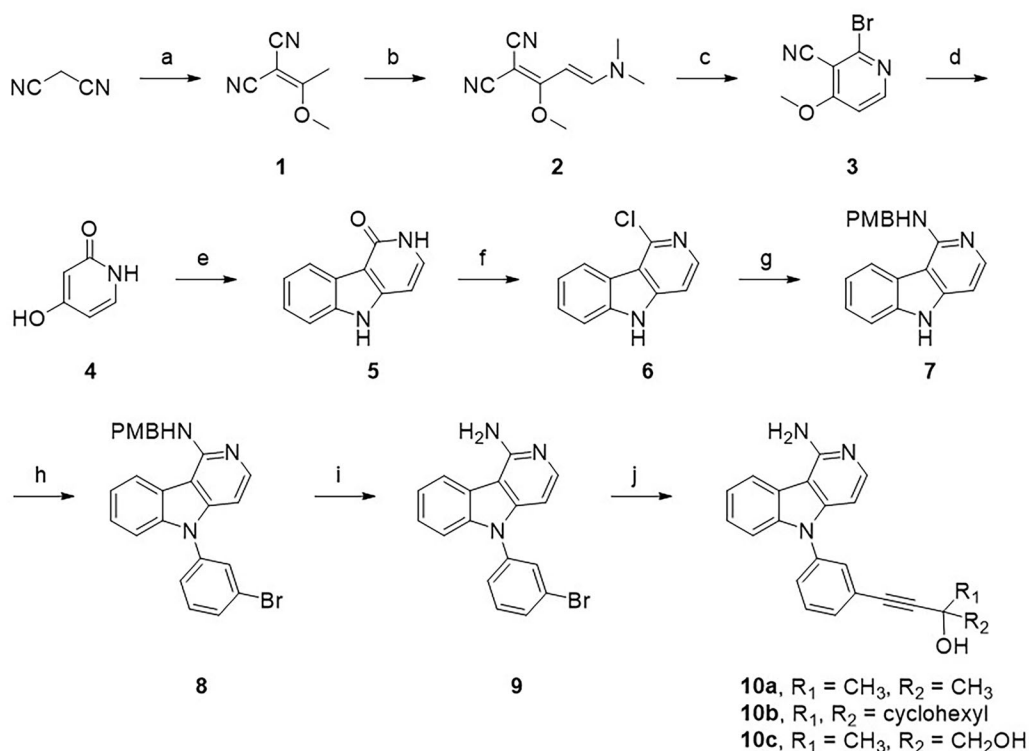
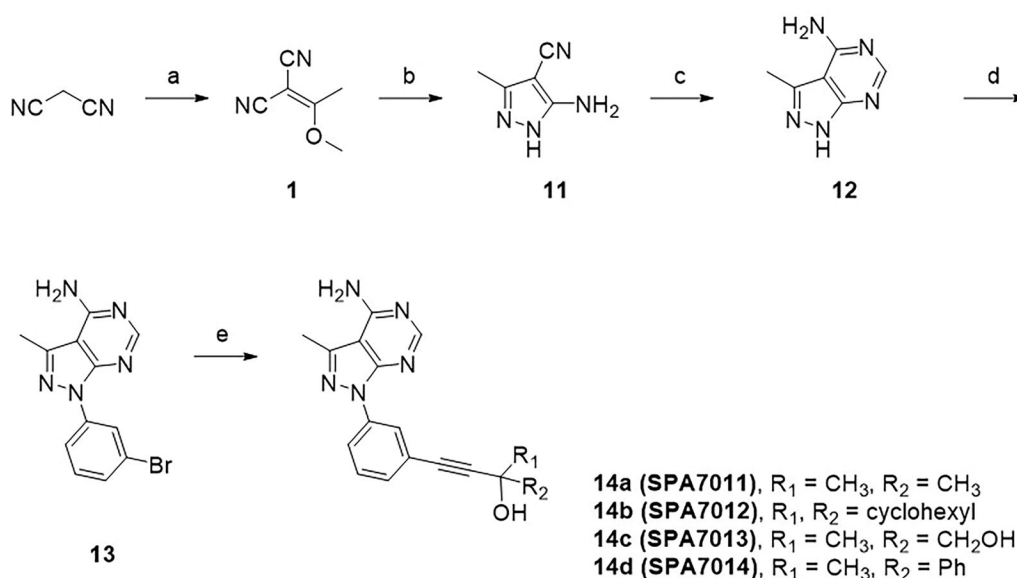


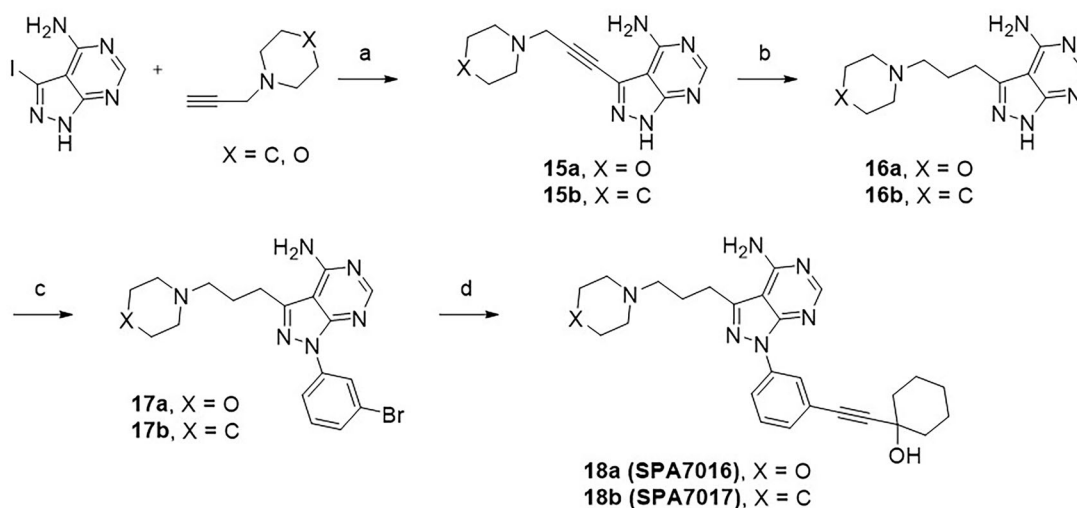
Figure 1. Drug design and identification of SPA7012 as PAK4 inhibitor. (A) Design strategy for novel PAK4 selective inhibitors. (B) Enzymatic IC₅₀ curves for SPA7012, SPA7016 and SPA7017. (C) Representative structure of pyrido[3,4-*d*]pyrimidine derivatives. (D) Predicted binding mode of SPA7012 (PDB code: 4O0V). Original ligand GNE-2861 (green) and SPA7012 (brown) are presented in the stick model. The hydrogen bonds are indicated as a green dashed line.



Scheme 1. Synthesis of 1-aminopyrido[4,3-*b*]indole derivatives. Reagents and conditions: (a) trimethyl orthoacetate, 100 °C; (b) DMF-DMA, MeOH, reflux; (c) 48% HBr, AcOH, room temperature; (d) conc. HCl, 160 °C; (e) phenylhydrazine, Ph₂O, 240 °C; (f) POCl₃, reflux; (g) *p*-methoxybenzylamine, 200 °C; (h) 1-bromo-3-iodobenzene, Cu, K₂CO₃, 18-crown-6, 1,2-dichlorobenzene, 180 °C; (i) TFA, 60 °C; and (j) *R*-prop-2-yn-1-ol, Pd(PPh₃)₂Cl₂, TEA/DMSO (2:1), 70 °C.



Scheme 2. Synthesis of the 4-aminopyrazolo[3,4-*d*]pyrimidine derivatives. Reagents and conditions: (a) trimethyl orthoacetate, 100 °C; (b) hydrazine monohydrate, EtOH, 80 °C; (c) formamide, 180 °C; (d) 1-bromo-3-iodobenzene, CuI, K₂CO₃, DMEDA, DMF, 110 °C; and (e) R-prop-2-yn-1-ol, Pd(PPh₃)₂Cl₂, TEA/DMSO (2:1), 70 °C.



Scheme 3. Synthesis of the 4-aminopyrazolo[3,4-*d*]pyrimidine derivatives with a solvent-accessible moiety. Reagents and conditions: (a) CuI, Pd(PPh₃)₄, TEA, DMF, 70 °C; (b) Pd/C, H₂, MeOH, room temperature; (c) 1-bromo-3-iodobenzene, CuI, K₂CO₃, DMEDA, DMF, 110 °C; and (d) 1-Ethynylcyclohexanol, Pd(PPh₃)₂Cl₂, TEA/DMSO (2:1), 70 °C.

pyrazolo[3,4-*d*]pyrimidine, were selected and designed as type I $1/2$ inhibitors.

A series of pyrido[4,3-*b*]indole derivatives were synthesised, as depicted in Scheme 1. Knoevenagel condensation of malononitrile with trimethyl orthoacetate yielded the enol ether.¹ Enamine² was obtained by treatment with *N,N*-dimethylformamide dimethyl acetal (DMF-DMA) and was converted to pyridine⁴ under acidic conditions. Fischer indole synthesis between 2,4-dihydroxypyridine⁴ and phenylhydrazine yielded a pyrido[4,3-*b*]indole moiety.⁵ The carbonyl group of pyridone⁵ was converted to chloropyridine⁶ by treatment with phosphoryl chloride, and the resulting chloropyridine was substituted with a *p*-methoxybenzyl (PMB) protected amine, which yielded aminopyridine.⁷ The Ullmann-type reaction of 5*H*-pyrido[4,3-*b*]indole with 1-bromo-3-iodobenzene resulted in *N*-phenyl-substituted pyridoindole,⁸ and deprotection of the PMB protective amine yield the free amine.⁹ The lipophilic groups targeting the back pocket were introduced by Sonogashira coupling

between aryl halide⁹ and alkynes, which produced the target compound **10**. Pyrazolo[3,4-*d*]pyrimidine derivatives were also synthesised as depicted in Scheme 2 and Scheme 3. The enol ether¹ synthesised from malononitrile was treated with hydrazine to obtain an aminopyrazole ring,¹¹ and subsequent cyclisation with formamide provided a 4-aminopyrazolo[3,4-*d*]pyrimidine scaffold.¹² Subsequent Ullmann reaction and Sonogashira coupling reaction provided the target compound **14**. A solvent-accessible moiety was then introduced to the 4-aminopyrazolo[3,4-*d*]pyrimidine backbone. Sonogashira coupling of 3-iodopyrazolo[3,4-*d*]pyrimidine with a substituted propyne introduced a solvent-accessible moiety, and hydrogenation yielded compound **16**. Similar to the previous compounds, Ullmann-type coupling and Sonogashira coupling reactions were performed sequentially to obtain the target compound **18**.

Synthesised compounds were evaluated for their *in vitro* PAK4 enzyme inhibitory activities. *In vitro* kinase assays were performed

Table 2. PAK4 enzyme inhibitory activity and calculated properties of synthesised compounds

Compound	PAK4 enzyme inhibition		clogP
	% inhibitory activity	IC ₅₀ (μM) ^b	
10a	32	ND	3.79
10b	54	34.0	5.10
10c	29	ND	2.66
14a	60	ND	1.25
14b	97	0.77	2.57
14c	36	ND	0.12
14d	65	ND	2.59
18a	88	9.92	2.57
18b	90	4.41	3.78

ND: not determined

^aRelative percentage inhibition at 20 μM of compounds with staurosporine, HotSpot kinase assay (Reaction Biology Corp.).

^bHotSpot kinase assay (Reaction Biology Corp.).

Table 3. PAK subtype selectivity of SPA7012

Subtype	% inhibitory activity ^a	IC ₅₀ (μM) ^b
PAK1	16	ND
PAK2	36	NA
PAK3	5	ND
PAK4	81	0.77
PAK5	52	>100
PAK6	36	NA

ND: not determined; NA: no activity

^aRelative percentage inhibition at 20 μM of compounds with staurosporine, HotSpot kinase assay (Reaction Biology Corp.).

^bHotSpot kinase assay (Reaction Biology Corp.).

using HotSpot kinase assays for relative enzyme inhibitory activity at a single concentration (20 μM) and IC₅₀ assessment at an ATP concentration of 10 μM (Figure 1(B)). The bicyclic pyrazolo[3,4-*d*]pyrimidine derivative (Figure 1(C)) showed increased activity than the tricyclic pyrido[4,3-*b*]indole derivative (Table 2). For the allosteric pocket binder, cyclohexyl group (SPA7012) was preferable to the smaller dimethyl (SPA7011) or hydroxymethyl group (SPA7013), and the aromatic ring (SPA7014) reduced activity compared to the saturated ring (SPA7012). *In vitro* enzyme IC₅₀ values appeared in the order of SPA7012, SPA7017, and SPA7016. Compound SPA7012 with a submicromolar IC₅₀ value was selected to evaluate subtype selectivity (Table 3), and showed enhanced selectivity for PAK4 (81% inhibition, 0.77 μM of IC₅₀) compared to PAK1 (16% inhibition) and PAK2 (36% inhibition, >100 μM of IC₅₀). Molecular docking analysis was performed on the human PAK4 catalytic domain structure complexed with GNE-2861 (PDB code: 4O0V). The binding pose of SPA7012 overlapped well with the crystal structure of GNE-2861, with the allosteric binder properly positioned in the specific back pocket. The oxygen atom in the tertiary alcohol of the hydrophobic allosteric binder formed hydrogen bonds with the backbone of Phe459 and the side chain of Glu366 (Figure 1(D)). The amine group and nitrogen atom in the pyrazolo[3,4-*d*]pyrimidine core scaffold also formed hydrogen bonds with Lue398 at the hinge region. Finally, SPA7012 was decided as a lead compound for further examination with satisfactory potency and subtype selectivity.

3.2. Intraperitoneal administration of SPA7012 attenuates hepatic I/R injury in mice

We first examined whether SPA7012 has an effect on liver damage in mice subjected to 1 h of ischaemia and 6 h or 24 h of reperfusion (Figure 2(A)). Liver injury as assessed by serum levels of AST and ALT was evident in mice undergoing I/R compared to those in sham-operated mice (Figure 2(B)). Administration of SPA7012

before and during I/R injury at a dose of 50 mg/kg significantly decreased both AST and ALT levels in I/R injured mice. Gross findings of liver morphology and liver necrosis were consistent with AST and ALT levels (Figure 2(C)). H&E staining revealed extensive hepatocellular necrosis in I/R-injured liver tissues compared with the sham group (Figure 2(C,D)). However, in SPA7012 treated mice, the area of necrosis was significantly smaller compared with the I/R group and there were considerable areas of normal liver structure.

Although the major cause of cell death during hepatic I/R injury is necrosis, apoptotic cell death was also observed during the injury process.^{19,20} The number of TUNEL-positive apoptotic cells was significantly larger in I/R-injured liver tissues while TUNEL-positive cells were rarely observed in the sham group (Figure 2(E)). Western blotting analyses showed increases in pro-apoptotic Bax and cleaved caspase-3, and a decrease in anti-apoptotic Bcl-2 in I/R injured livers (Figure 2(F)). When mice were treated with SPA7012, a significant reduction in TUNEL-positive cells and concordant changes in apoptotic proteins were observed. Together, these results indicate that SPA7012 has protective effects against hepatocellular damage upon I/R injury.

3.3. SPA7012 reduces oxidative stress in mice with I/R injury

To determine whether SPA7012 provided protection against I/R injury, we measured oxidative stress markers in liver tissues. MDA levels (an indicator of lipid peroxidation) were greatly increased in I/R injured liver tissues compared with the sham group (Figure 3(A)). Conversely, I/R caused a significant suppression of antioxidant GSH levels in liver tissues (Figure 3(B)). Immunostaining of liver tissues with 4-HNE revealed an increase of lipid peroxidation subsequent to I/R injury (Figure 3(C)). However, SPA7012 treatment reversed changes caused by I/R; the serum level of MDA was significantly lower, hepatic levels of GSH were significantly higher, and 4-HNE-positive cells were significantly lower in the SPA7012 group than the I/R group.

Our previous study found that PAK4 phosphorylates Nrf2 at Thr369, which triggers its nuclear export and subsequent proteasomal degradation in the cytoplasm.⁹ Therefore we investigated whether SPA7012 could affect subcellular localisation, protein stability, and transcriptional activity of Nrf2. Co-IP analysis after the overexpression of Nrf2 and PAK4 in HEK293T cells showed that SPA7012 effectively inhibited PAK4-mediated phosphorylation of Nrf2 at threonine residue (Figure 3(D)). Consistently SPA7012 treatment increased the nuclear level of Nrf2 in I/R injured liver tissues (Figure 3(E)) and Nrf2 transcriptional activity in HEK293T cells (Figure 3(F)). qPCR and Western blotting analyses further confirmed the enhanced transcriptional activity of Nrf2 by SPA7012 treatment in I/R injured liver tissues (Figure 3(G,H)). These results indicate that SPA7012 exhibits hepatoprotective effects against I/R injury through stabilising Nrf2 protein and enhancing antioxidant protein expression.

3.4. SPA7012 suppresses inflammation in mice with I/R injury

Hepatic I/R is also characterised by sterile inflammation, in which resident Kupffer cells are activated or immune cells (monocytes and neutrophils) are recruited to the liver tissues in response to hepatocyte death. We first immunostained liver tissues to evaluate the degree of inflammation 24 h after reperfusion. The number of F4/80-positive macrophages and Ly6G-positive neutrophils were both notably increased during hepatic I/R (Figure 4(A)), indicating inflammation in the liver. The levels of proinflammatory cytokines/

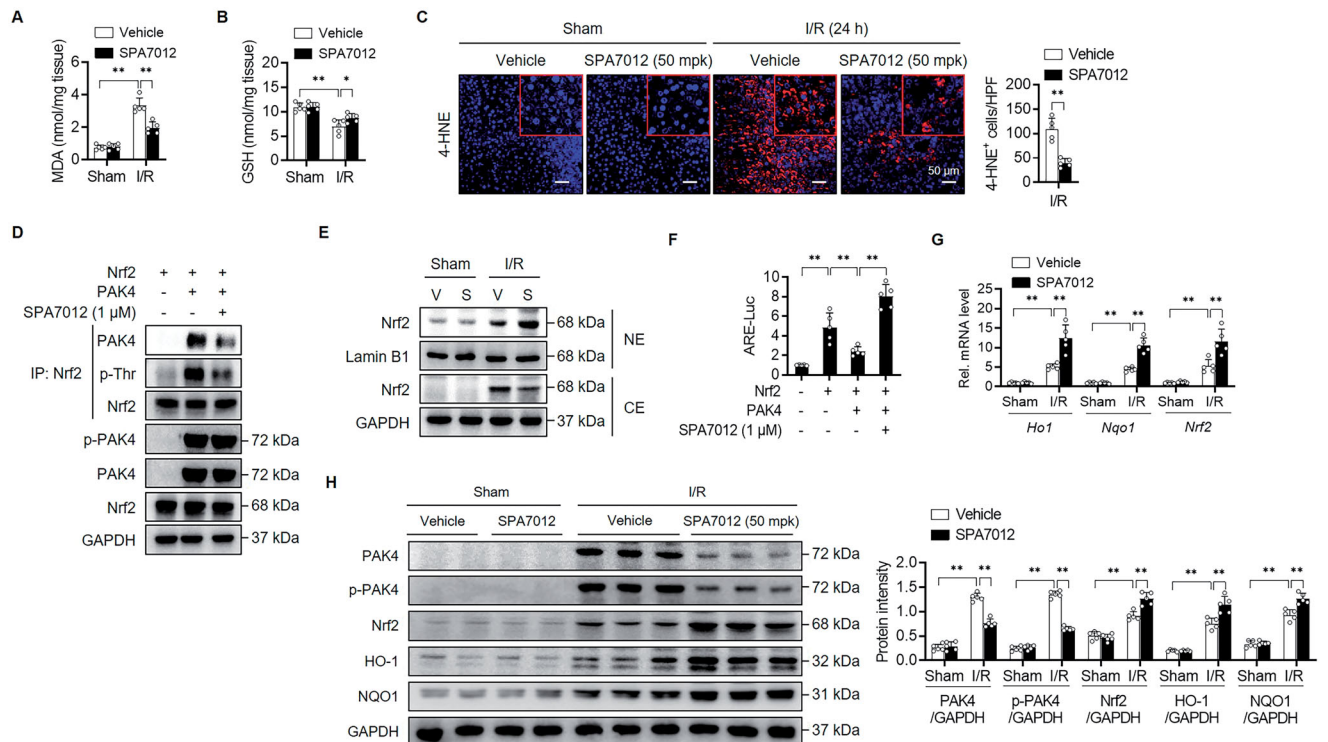
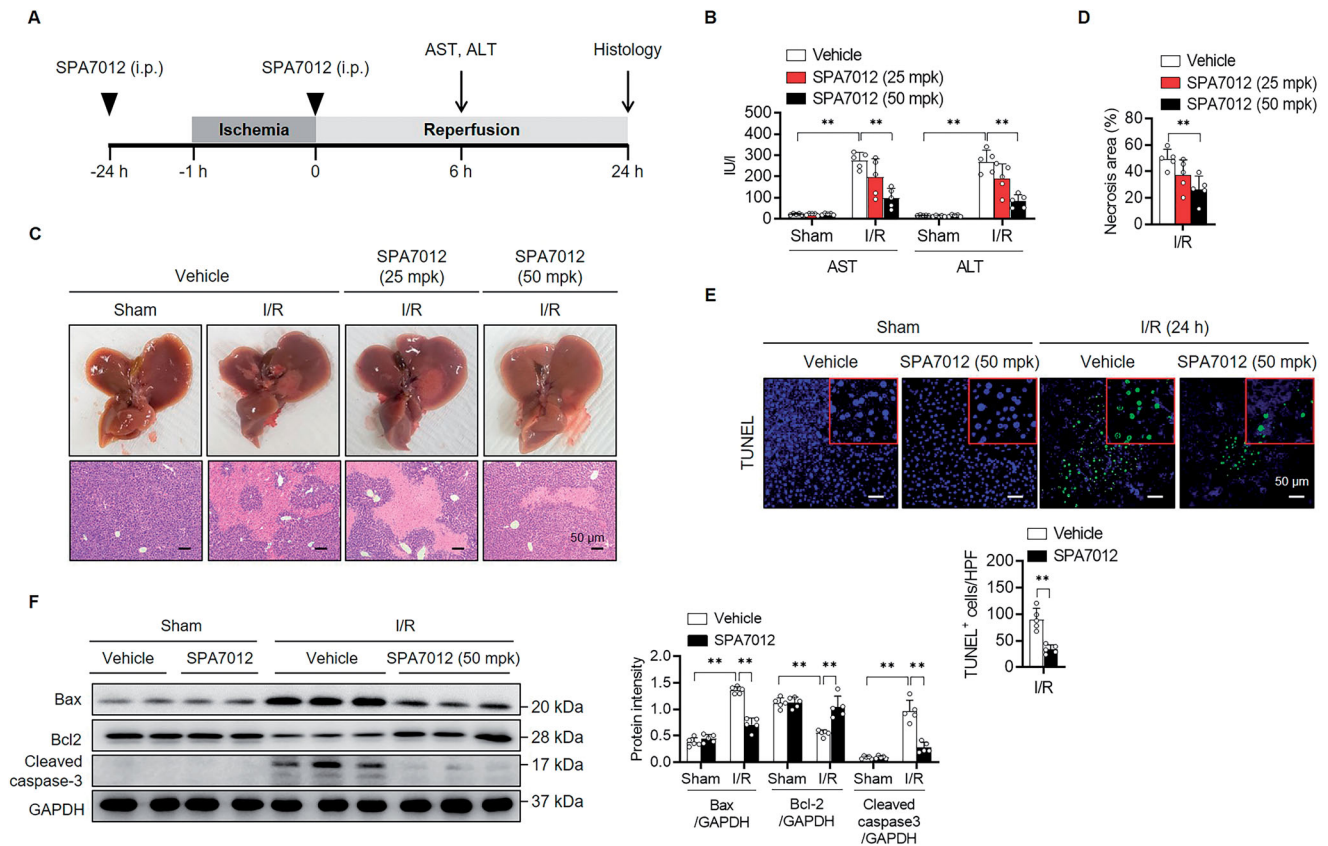


Figure 3. Attenuation of I/R-induced oxidative stress by SPA7012. (A and B) Hepatic levels of malondialdehyde (MDA) and glutathione (GSH) ($n=5$). (C) Immunohistochemical staining for 4-hydroxynonenal (4-HNE) of liver tissues ($n=5$). (D) A co-IP analysis in HEK293T cells after 24 h transfection. (E) Nrf2 protein levels in nuclear (NE) and cytosolic extracts (CE) of I/R injured liver tissues. (F) ARE Luciferase activity in HEK293T cells after 24 h transfection ($n=5$). (G and H) Nrf2 and its target gene levels in liver tissues ($n=5$). Values are the mean \pm SD. ** $p < 0.01$. I/R, ischaemia-reperfusion; HPF, high-power field; V, vehicle; S, SPA7012 50 mg/kg.

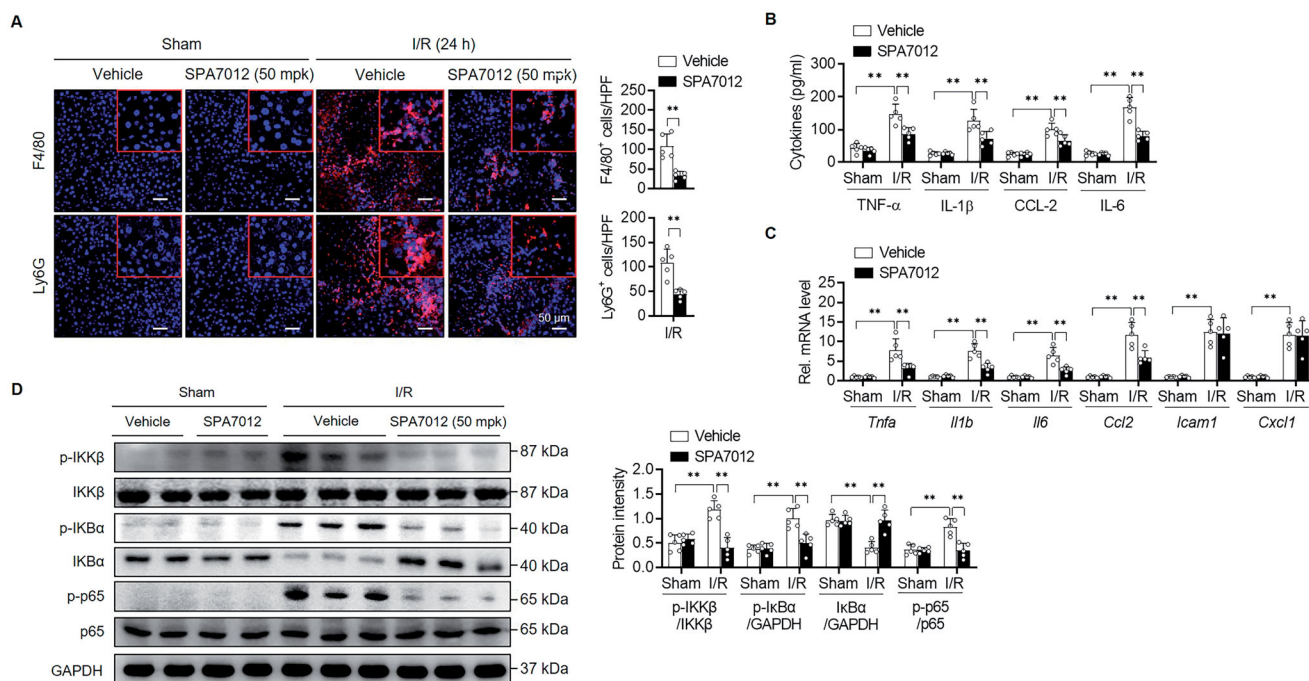


Figure 4. Attenuation of I/R-induced inflammation by SPA7012. (A) Immunofluorescence staining and quantification of F4/80-positive macrophages and Ly6G-positive neutrophils in liver tissues ($n = 5$). (B and C) The protein and mRNA levels of pro-inflammatory cytokines/chemokine in serum and liver tissues ($n = 5$). (D) Protein levels of NF- κ B signalling pathway ($n = 5$). Values are the mean \pm SD. ** $p < 0.01$. HPF: high-power field.

chemokines (TNF- α , IL-1 β , IL-6, and CCL-2) in the serum and corresponding mRNA levels in the liver were also significantly increased by I/R injury (Figure 4(B,C)). However, the treatment of mice with SPA7012 decreased inflammatory cell infiltration and cytokine production. As NF- κ B is closely correlated with inflammatory cytokine production, we analysed the NF- κ B signalling pathway by Western blotting. We found that SPA7012 treatment substantially decreased phosphorylation levels of IKK β and p65, and increased protein levels of I κ B α compared to those of sham mice (Figure 4(D)). These results confirm that suppression of inflammation utilising SPA7012 may further provides to protection against I/R injury.

3.5. SPA7012 suppresses H/R-induced apoptotic cell death and inflammation in hepatocytes

In order to simulate hepatic I/R injury, we established an *in vitro* H/R-induced hepatocellular damage model (Figure 5(A)). SPA7012 at a concentration of less than 1 μ M had little effect on cell viability (Figure 5(B)). Exposure to H/R significantly increased LDH release from primary hepatocytes compared with the normoxic group. However, when the cells were cultured with SPA7012 at 1 μ M concentration before exposure to reoxygenation injury, cell damage was markedly decreased compared to only H/R (Figure 5(C)). Based on these results, 1 μ M of SPA7012 was selected for the following experiments. Similar to I/R injury, H/R injury increased apoptotic cell death (Figure 5(D,E)), oxidative stress (Figure 5(F,G)), and cytokine release in primary hepatocytes (Figure 5(H,I)), while SPA7012 treatment resulted in a decrease of these negative responses. Again, SPA7012 treatment decreased phosphorylation levels of IKK β and p65, and increased protein levels of I κ B α compared to control group (Figure 5(J)).

4. Discussion

In the present study, we showed the hepatoprotective effects of PAK4 inhibitor SPA7012 in a mouse model of hepatic I/R. This protection confirms the results of our previous study⁹ and is attributed to Nrf2 protein stabilisation by PAK4 inhibitor and its anti-inflammatory effect.

Through *in silico* fragment screening, privileged bicyclic adenine pocket-binding scaffolds were selected to secure PAK4 specific inhibitors. Novel pyrazolo[3,4-*d*]pyrimidine derivatives with an allosteric back pocket binder were discovered as a type I $1/2$ inhibitor, while the aforementioned CZh-226 was classified as a type I inhibitor. The type I inhibitors bind to the adenine site of the ATP pocket, with the Asp-Phe-Gly (DFG) motif of the activation loop adopting an 'in' conformation. Type II inhibitors bind to both the adenine site and an adjacent allosteric pocket created by accepting a DFG 'out' conformation. It is subdivided into the type I $1/2$ inhibitors, which bind to an inactive kinase with a DFG 'in' structure.²¹ For kinome selectivity, type I $1/2$ inhibitors are advantageous.²² Based on the number of identified kinase targets, type I $1/2$ inhibitors indicate higher target selectivity (69%) compared to type I inhibitors (35%). Among the synthesised compounds, a pyrazolo[3,4-*d*]pyrimidine compound SPA7012 showed successful potency with an IC₅₀ value of 0.77 μ M and PAK4 selectivity.

During the process of hepatic I/R injury, redox homeostasis is impaired and large quantities of ROS are produced, resulting in protein and lipid peroxidation and DNA damage. Studies have demonstrated that the activation of Nrf2 is beneficial in maintaining integrity and function of liver tissues.^{4,23} Our recent study uncovered the regulation of Nrf2 protein stability by PAK4. Upon hepatic I/R injury, PAK4 is transcriptionally activated via HIF-1 α . The induced PAK4 directly phosphorylates Nrf2 at T369, which leads to the nuclear export and proteasomal degradation of Nrf2. In contrast, genetic ablation of *Pak4* in hepatocytes stabilises Nrf2 and induces antioxidant enzymes such as HO-1 and NQO1, preventing oxidative damage.⁹ In the current study, pre-treatment of

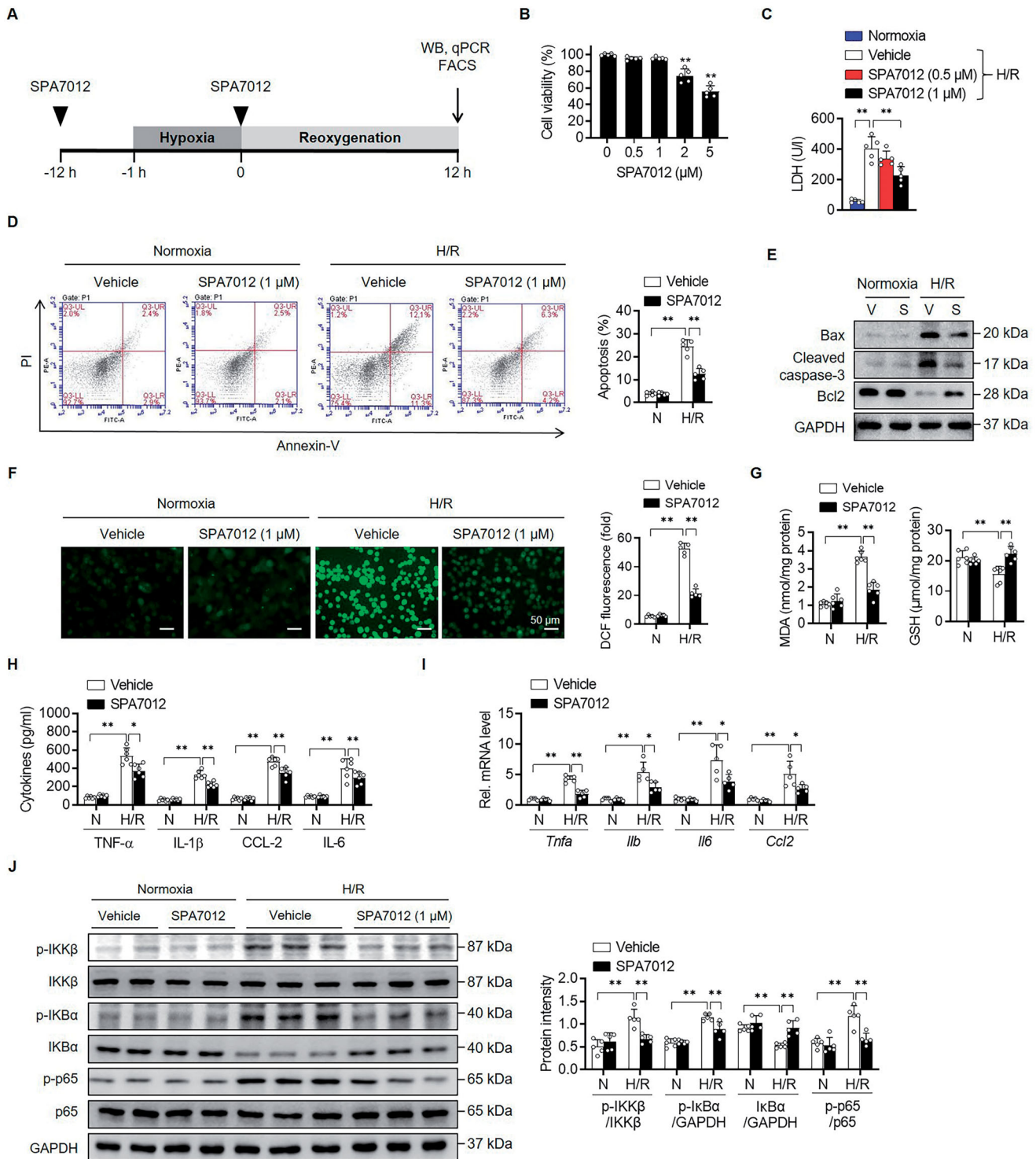


Figure 5. Attenuation of H/R-induced apoptotic cell death and cytokine production by SPA7012. (A) Schematic diagram of treatment of SPA7012 to primary hepatocytes. (B) MTT assay for cell viability ($n=5$). (C) Lactate dehydrogenase (LDH) release from primary hepatocytes after 12 h reoxygenation ($n=5$). (D and E) Analysis of apoptotic cell death by Annexin-V staining and Western blotting ($n=5$). (F and G) Reactive oxygen species levels assessed using fluorescence microscopy following the changes in DCF fluorescence and colorimetric analysis of MDA and GSH ($n=5$). (H and I) The protein and mRNA levels of pro-inflammatory cytokines/chemokine in culture media and hepatocytes ($n=5$). (J) Protein levels of NF- κ B signalling pathway ($n=5$). Values are the mean \pm SD. * $p < 0.05$ and ** $p < 0.01$. H/R: hypoxia-reoxygenation.

mice twice with SPA7012 at 50 mg/kg considerably increased post I/R protein levels of total and nuclear Nrf2 as well as its target genes in liver tissues. The subject study indicated that SPA7012 treatment resulted in reduced oxidative injury in I/R exposed mice liver.

The phosphorylation of Nrf2 is also regulated by several other kinases. The best characterised regulator is the PI3K-Akt-GSK-3 β pathway as GSK-3 β phosphorylates Nrf2, resulting in its nuclear exclusion and functional inhibition.⁷ Akt phosphorylates and thus inhibits GSK-3 β activity, positively regulating Nrf2.²⁴ In addition,

PI3K/Akt blockade impedes Nrf2 transcriptional activity and aggravates I/R damage.²⁵ Recently, we reported PAK4 phosphorylates PPAR γ as capable of inducing PTEN, a lipid phosphatase that opposes the action of the PI3K-Akt pathway in myotoxin-treated myocytes.²⁶ Thus, the question arises as to whether Nrf2 transcriptional activation is affected by PI3K-Akt-GSK-3 β signalling in our model. Our results showed no changes to total- and phospho-protein levels of PPAR γ , PTEN, Akt, and GSK-3 β following SPA7012 treatment (data not shown), indicating that Nrf2 activation and concomitant hepato-protection by SPA7012 in I/R injury are not related to the Akt/GSK-3 β dependent pathway.

We found in this study that SPA7012 treatment markedly suppressed canonical NF- κ B signalling, as it reduced the phosphorylation of IKK β /p65 and the transcription of pro-inflammatory cytokines and adhesion molecules. This was coupled with a drastic reduction of macrophage and neutrophil infiltration in post-ischemic liver tissues. Given that NF- κ B plays a critical role in regulating inflammation, oxidative stress, cell death, and cell survival,²⁷ we suggest that inhibition of NF- κ B signalling by SPA7012 may represent a significant role in protection from I/R injury. Related to these findings, PAK4 is known to activate canonical NF- κ B signalling (essentially via RELA, NF- κ B p65 subunit) in cultured cancer cells,^{28–30} which contribute to cell proliferation and cell migration. Although we do not provide the direct evidence that SPA7012 inhibited NF- κ B signalling through PAK4 inhibition, this study strongly suggests that PAK4 inhibition exerts an anti-inflammatory property during hepatic I/R.

PAK4 has been shown to promote cell proliferation and suppress apoptosis in many cancer models.^{28,30,31} However this conclusion is not in agreement with our model, where PAK4 inhibition resulted in strong anti-apoptotic effects, as evidenced by a decreased number of TUNEL-positive cells with concomitant decreased hepatic levels of pro-apoptotic proteins. A causal link may exist between NF- κ B activation and the reduction in apoptotic cell numbers in hepatic tissue, as NF- κ B activation has been considered a key process involved in apoptotic cell death during reperfusion.³² These results concur with our recent study showing that the *Pak4* deletion in hepatocytes suppresses both NF- κ B and TUNEL-positive cells in liver tissues.⁹ Similarly, our previous report also shows that NF- κ B suppression by A20 decreases apoptotic cell numbers in liver tissues after hepatic I/R.¹⁵ Thus, the inhibition of PAK4 has the ability to suppress apoptotic cell death following hepatic I/R.

In summary, this study demonstrates that pharmacological inhibition of PAK4 by SPA7012 ameliorates hepatic I/R injury in mice, which occurs as a result of stabilising Nrf2 and enhancing antioxidant capacity. Additionally, these results reveal the anti-apoptotic and anti-inflammatory properties of SPA7012 in liver tissues. These findings can be used to broaden our understanding of PAK4 on the pathogenesis of hepatic I/R, and support PAK4 as a new molecular target for therapeutic approaches to remedy I/R injuries in another organs.

Acknowledgements

The authors thank the Writing Center at Jeonbuk National University for its skilled proofreading service.

Author contributions

EL and RJ synthesised the PAK4 inhibitor. YM performed the *in vitro* and *in vivo* experiments. EJB and BHP designed the

experiments, interpreted the data, and wrote the manuscript. All authors reviewed the manuscript.

Disclosure statement

RJ, EL, EJB, and BHP are planning to apply the PAK4-specific inhibitor, SPA7012, for a patent. The remaining authors have no conflict of interest to declare.

Funding

This work was supported by the National Research Foundation of Korea [grant number 2017R1A5A2015061], [grant number 2019R1F1A1057386], [grant number 2021R1A2C1003358], [grant number 2022M3E5F2017607] and Korea Drug Development Fund [grant number HN21C0447], which are funded by the Korean government.

References

1. Eltzschig HK, Eckle T. Ischemia and reperfusion—from mechanism to translation. *Nat Med* 2011;17:1391–401.
2. Konishi T, Lentsch AB. Hepatic ischemia/reperfusion: mechanisms of tissue injury, repair, and regeneration. *Gene Expr* 2017;17:277–87.
3. Lentsch AB, Kato A, Yoshidome H, et al. Inflammatory mechanisms and therapeutic strategies for warm hepatic ischemia/reperfusion injury. *Hepatology* 2000;32:169–73.
4. Kudoh K, Uchinami H, Yoshioka M, et al. Nrf2 activation protects the liver from ischemia/reperfusion injury in mice. *Ann Surg* 2014;260:118–27.
5. Lee LY, Harberg C, Matkowskyj KA, et al. Cell-specific overactivation of nuclear erythroid 2 p45-related factor 2-mediated gene expression in myeloid cells decreases hepatic ischemia/reperfusion injury. *Liver Transpl* 2016;22:1115–28.
6. Xu D, Xu M, Jeong S, et al. The role of Nrf2 in liver disease: novel molecular mechanisms and therapeutic approaches. *Front Pharmacol* 2018;9:1428.
7. Salazar M, Rojo AI, Velasco D, et al. Glycogen synthase kinase-3 β inhibits the xenobiotic and antioxidant cell response by direct phosphorylation and nuclear exclusion of the transcription factor Nrf2. *J Biol Chem* 2006;281:14841–51.
8. Liu T, Lv YF, Zhao JL, et al. Regulation of Nrf2 by phosphorylation: consequences for biological function and therapeutic implications. *Free Radic Biol Med* 2021;168:129–41.
9. Mao Y, Han CY, Hao L, et al. PAK4 inhibition protects against liver ischemia/reperfusion injury: role of Nrf2 phosphorylation. *Hepatology* 2022;76:345–56.
10. Murray BW, Guo C, Piraino J, et al. Small-molecule p21-activated kinase inhibitor PF-3758309 is a potent inhibitor of oncogenic signaling and tumor growth. *Proc Natl Acad Sci U S A* 2010;107:9446–51.
11. Senapedis W, Crochiere M, Baloglu E, Landesman Y. Therapeutic potential of targeting PAK signaling. *Anticancer Agents Med Chem* 2016;16:75–88.
12. Rudolph J, Crawford JJ, Hoefflich KP, Wang W. Inhibitors of p21-activated kinases (PAKs). *J Med Chem* 2015;58:111–29.
13. Abu Aboud O, Chen CH, Senapedis W, et al. Dual and specific inhibition of NAMPT and PAK4 by KPT-9274 decreases kidney cancer growth. *Mol Cancer Ther* 2016;15:2119–29.

14. Hao C, Zhao F, Song H, et al. Structure-based design of 6-chloro-4-aminoquinazoline-2-carboxamide derivatives as potent and selective p21-activated kinase 4 (PAK4) inhibitors. *J Med Chem* **2018**;61:265–85.
15. Yu J, Lee HS, Lee SM, et al. Aggravation of post-ischemic liver injury by overexpression of A20, an NF-kappaB suppressor. *J Hepatol* **2011**;55:328–36.
16. Zhang EY, Ha BH, Boggon TJ. PAK4 crystal structures suggest unusual kinase conformational movements. *Biochim Biophys Acta Proteins Proteom* **2018**;1866:356–65.
17. Staben ST, Feng JA, Lyle K, et al. Back pocket flexibility provides group II p21-activated kinase (PAK) selectivity for type I 1/2 kinase inhibitors. *J Med Chem* **2014**;57:1033–45.
18. Fabbro D, Ruetz S, Buchdunger E, et al. Protein kinases as targets for anticancer agents: from inhibitors to useful drugs. *Pharmacol Ther* **2002**;93:79–98.
19. Wang J, Koh HW, Zhou L, et al. Sirtuin 2 aggravates post-ischemic liver injury by deacetylating mitogen-activated protein kinase phosphatase-1. *Hepatology* **2017**;65:225–36.
20. Bae UJ, Yang JD, Ka SO, et al. SPA0355 attenuates ischemia/reperfusion-induced liver injury in mice. *Exp Mol Med* **2014**;46:e109.
21. Zuccotto F, Ardini E, Casale E, Angiolini M. Through the "gatekeeper door": exploiting the active kinase conformation. *J Med Chem* **2010**;53:2681–94.
22. Roskoski R. Jr., Properties of FDA-approved small molecule protein kinase inhibitors: a 2020 update. *Pharmacol Res* **2020**;152:104609.
23. Yi Z, Deng M, Scott MJ, et al. Immune-responsive gene 1/Itaconate activates nuclear factor erythroid 2-related factor 2 in hepatocytes to protect against liver ischemia-reperfusion injury. *Hepatology* **2020**;72:1394–411.
24. Xin Y, Bai Y, Jiang X, et al. Sulforaphane prevents angiotensin II-induced cardiomyopathy by activation of Nrf2 via stimulating the Akt/GSK-3 β /Fyn pathway. *Redox Biol* **2018**;15:405–17.
25. Ke B, Shen XD, Zhang Y, et al. KEAP1-NRF2 complex in ischemia-induced hepatocellular damage of mouse liver transplants. *J Hepatol* **2013**;59:1200–7.
26. Mao Y, Han CY, Hao L, et al. p21-activated kinase 4 phosphorylates peroxisome proliferator-activated receptor γ and suppresses skeletal muscle regeneration. *J Cachexia Sarcopenia Muscle* **2021**;12:1776–88.
27. Morgan MJ, Liu ZG. Crosstalk of reactive oxygen species and NF-kappaB signaling. *Cell Res* **2011**;21:103–15.
28. Li X, Minden A. PAK4 functions in tumor necrosis factor (TNF) α -induced survival pathways by facilitating TRADD binding to the TNF receptor. *J Biol Chem* **2005**;280:41192–200.
29. Ryu BJ, Lee H, Kim SH, et al. PF-3758309, p21-activated kinase 4 inhibitor, suppresses migration and invasion of A549 human lung cancer cells via regulation of CREB, NF-kappaB, and beta-catenin signalings. *Mol Cell Biochem* **2014**;389:69–77.
30. Li Q, Zhang X, Wei N, et al. p21-activated kinase 4 as a switch between caspase-8 apoptosis and NF-kappaB survival signals in response to TNF- α in hepatocarcinoma cells. *Biochem Biophys Res Commun* **2018**;503:3003–10.
31. Wang M, Gao Q, Chen Y, et al. PAK4, a target of miR-9-5p, promotes cell proliferation and inhibits apoptosis in colorectal cancer. *Cell Mol Biol Lett* **2019**;24:58.
32. Malhi H, Gores GJ, Lemasters JJ. Apoptosis and necrosis in the liver: a tale of two deaths? *Hepatology* **2006**;43:S31–S44.